

Surgical Aggregation: A Collaborative Learning Framework for Harmonizing Distributed Medical Imaging Datasets with Diverse Tasks

Pranav Kulkarni¹, Adway Kanhere¹, Paul Yi¹, Vishwa Parekh^{1*}

¹University of Maryland Medical Intelligent Imaging (UM2ii) Center, University of Maryland School of Medicine, Baltimore, MD.

*Corresponding author(s). E-mail(s): vparekh@som.umd.edu;
 Contributing authors: pkulkarni@som.umd.edu; akanhere@som.umd.edu;
pyi@som.umd.edu;

Abstract

Large-scale chest x-ray datasets have been curated for the detection of abnormalities using deep learning, with the potential to provide substantial benefits across many clinical applications. However, each dataset focuses only on detecting a subset of findings that can be simultaneously present in a patient, thereby limiting its clinical utility. Therefore, data harmonization is crucial to leverage these datasets in aggregate to train clinically-useful, robust models with a complete representation of all abnormalities that may occur within the thorax. To that end, we propose surgical aggregation, a collaborative learning framework for harmonizing and aggregating knowledge from distributed heterogeneous datasets with partial disease annotations. We evaluate surgical aggregation across synthetic iid datasets and real-world large-scale non-iid datasets with partial annotations. Our results indicate that surgical aggregation significantly outperforms current strategies, has better generalizability, and has the potential to revolutionize the development clinically-useful models as AI-assisted disease characterization becomes a mainstay in radiology.

Keywords: Deep learning, federated learning, surgical aggregation, data harmonization, chest x-ray, classification.

Main

Chest X-Ray (CXR) is the most commonly ordered medical imaging study globally and is critical for screening many life threatening conditions. As a result, many large-scale curated CXR datasets have been released for the purpose of training clinically-useful deep learning models with expert-level detection of diseases in the thorax [1–4]. Unfortunately, due to the nature of curating large-scale datasets, each dataset focuses

only on detecting a subset of findings that can be simultaneously present in a patient, thereby limiting its clinical utility. Since annotations present in one dataset may not be present in another, these datasets are incomplete due to this inherent label heterogeneity. Similarly, each dataset is acquired and curated using different imaging equipment, acquisition parameters, image processing techniques and label extraction methods. Due to these differences, these datasets are heterogeneous and not independent and identically distributed (iid).

This can lead to domain shift as models trained on one dataset may not generalize well on an unseen dataset sourced from another institution [5–9].

For example, the NIH Chest X-Ray 14 [4] and CheXpert [1] datasets are heterogeneous due to inherent differences in their acquisition and curation processes. Similarly, both datasets focus on different disease labels, thus making them incomplete despite sharing seven disease labels. To leverage knowledge from these datasets would require training models separately on each dataset. This would result in an ever increasing number of models as more datasets get curated and released, thus, making this approach impractical. Furthermore, individually trained models may not generalize well to unseen data distributions in the real-world due to domain shift, thus, limiting their utility in the clinical setup [6, 8, 10]. Similarly, naively training a model on these datasets in aggregate across all observed disease labels without data harmonization could lead to an incomplete and inaccurate representation of the data and disease label distributions due to domain shift.

Different groups have explored the idea of building generalized multi-task deep learning models for different applications by leveraging multiple datasets in aggregate. Cohen et al. [11] compared the performance of CXR detection models trained on multiple datasets in aggregate with models trained separately on individual datasets. They observed that models trained on multiple datasets in aggregate demonstrated higher performance and generalized better to unseen datasets, compared to models trained individually. However, aggregating datasets in a centralized training setup is not only expensive due to storage and bandwidth constraints, but also practically challenging due to patient data privacy concerns. Therefore, federated learning (FL) was proposed as promising collaborative machine learning paradigm that approaches this problem from a decentralized and distributed approach. Consisting of a central server with multiple participating clients, FL can train a global model on distributed datasets by aggregating knowledge learned by local models at each client. In the realm of medical imaging, FL has enabled training of large-scale global models using homogeneous data spread across multiple institutions without

sharing sensitive patient data [12–14]. However, majority of the datasets being curated across the world are non-iid, heterogeneous and focus on similar but different tasks. This poses a significant challenge for the federated approach, as local models may differ significantly from each other. As a result, tackling non-iid data with domain shift and incomplete/partial labels is crucial. Consequently, different strategies and heuristics have been proposed in the literature for aggregating knowledge from heterogeneous non-iid datasets and tackle domain shift [10, 15–19]. However, this is a recent and relatively unexplored field in deep learning for medical imaging.

Knowledge distillation has emerged as a popular technique across multiple domains to tackle data heterogeneity [16, 17, 19–21]. An ensemble attention distillation based FL approach was explored to harmonize the NIH and CheXpert datasets, demonstrating the ability to train a global model with 14 disease labels, with 12 from CheXpert and eight from the NIH dataset [17]. However, the proposed approach required an external dataset and worked only in a multi-class scenario i.e. a patient could not be diagnosed with more than one disease, making it practically challenging and not clinically-useful. Alternatively, Arasteh et al. [15] proposed an approach involving aggregating only the network backbone during FL training. However, this approach involved further training of the local models post-federation resulting in different local models optimized for their respective tasks as opposed to a single multi-task global model. Meanwhile, other groups have pin-pointed the source of domain shift in the federated setup to the presence of batch normalization (BN) layers, a core element within model architectures [10, 19, 22, 23]. By normalizing, recentering, and rescaling the layer inputs, BN aimed to ensure rapid and stable model convergence by learning a moving mean of the training data statistics [24]. However, the naïve aggregation of BN statistics – in the case of FedAvg, the de-facto strategy for model weight aggregation in FL – was demonstrated to yield a sub-optimal solution with distributed non-iid data due to domain shift [19, 22, 25]. Consequently, FedBN was proposed as a solution to ensure model convergence using distributed non-iid data by preventing the aggregation of BN layers and allowing each local model to adapt its BN statistics to its training

data [19]. However, recent literature has indicated that despite FedBN demonstrating superior performance over FedAvg on non-iid data, it results in a sub-optimal solution in scenarios with partial labels and has limited clinical utility due to its inherent inability to learn a global model [10, 23]. More recently, FedFBN has been proposed to address these limitations by drawing inspiration from transfer learning. By using pre-trained networks and freezing the BN statistics during training, FedFBN yields significant improvements over other aggregation strategies in scenarios with distributed non-iid data with partial labels [10].

Data and label harmonization are two sides of the same coin. While significant advancements in recent literature have aimed to address data heterogeneity, it is evident that the presence of incomplete annotations in medical imaging data is an impediment to leveraging these large-scale heterogeneous datasets in aggregate across both federated and centralized setups. Most approaches focus on either detecting either (1) the presence of an abnormality i.e. normal vs. not normal, or (2) the disease labels shared across all datasets [8, 9, 11, 26]. As a result, the clinical utility of training a model across multiple datasets in aggregate is limited without data and disease label harmonization. Therefore, a method to harmonize and aggregate knowledge from distributed datasets with partial annotations could revolutionize the development of clinically-relevant deep learning models. To that end, we propose surgical aggregation, a collaborative learning framework for harmonizing and aggregating knowledge from distributed heterogeneous datasets with partial disease annotations into a global deep learning model. We utilize surgical aggregation in the central server to aggregate relevant knowledge coming in from each client to effectively learn different tasks across distributed heterogeneous datasets. Our proposed framework is (1) model and task-agnostic, (2) semi-supervised i.e. does not require any additional external dataset for validation during the training process, (3) capable of training a global model across all observed disease labels, and (4) can work in a federated and centralized setup.

In other words, surgical aggregation enables each participating client to train a robust, well generalizable model on client-specific tasks using knowledge learned by other clients performing

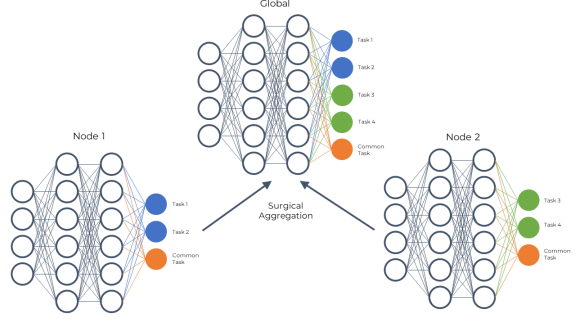


Fig. 1 An overview of the surgical aggregation framework.

similar tasks in aggregate, while enabling access to a larger set of different diagnostic tasks via the global model. Let's consider a consortium of two institutions, where the first focuses on the segmentation of multiple tumors within the abdomen (liver, spleen, etc.), while another focuses solely on liver tumors. Suppose, in the future, the second institution intends to expand their diagnostic capabilities to other organs. Due to domain shift, this would require the second institution to retrain a new model in both centralized and federated setups. In stark contrast, surgical aggregation addresses this limitation by training a global model across all tasks in aggregate. It enables an ad hoc expansion of diagnostic capabilities at the second institution by "importing" tasks learned by the global model without the need for retraining. Furthermore, this capability enables a new institution to join this consortium and simply import all relevant diagnostic tasks from the global model for their clinical application without the need for training any model. As AI-assisted disease characterization becomes a mainstay in radiology, we demonstrate how surgical aggregation provides a framework for greater multi-institutional collaboration to train large-scale clinically-useful models in aggregate, while reducing the barrier to entry for other institutions.

Results

In this work, we evaluated surgical aggregation across two experiments for the detection of abnormalities in CXRs. In the first experiment, we utilized synthetic iid datasets sampled from the NIH dataset to perform analytical experiments to evaluate the performance of surgical aggregation

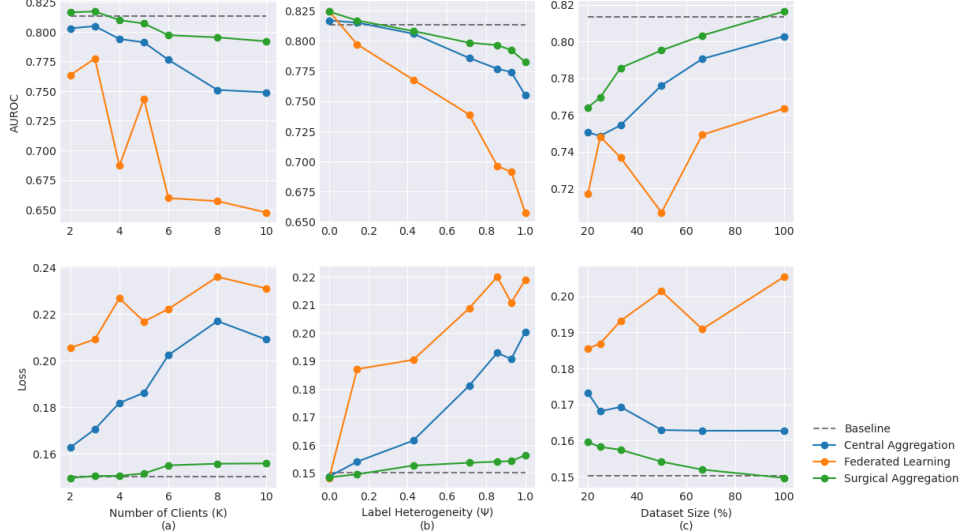


Fig. 2 Model metrics on the held-out NIH test set when evaluating the effect of (a) number of clients (K), (b) label heterogeneity (ψ), and (c) dataset size (N).

across varying data and disease label heterogeneity and dataset size. In the second experiment, we surgically aggregated and harmonized the NIH and CheXpert datasets, two real-world non-iid datasets with partial labels, into a global model with the capability to classify all 20 observed disease labels. Across both experiments, we compared surgical aggregation with two other strategies for training models in aggregate with the presence of partial annotations:

1. Central Aggregation, where contributing datasets are assumed to be locally available and the model is trained in a centralized setup across all observed labels.
2. Federated Learning, where contributing datasets are distributed across multiple clients and the model is trained using the conventional FL approach where the entire network is aggregated across all participating clients without surgical aggregation.

Analytical experiments with synthetic iid datasets

For our first set of experiments, we sampled multiple synthetic iid datasets from the NIH dataset to simulate different number of clients as well as different levels of data and label heterogeneity. The goal of these experiments was to explore the

scalability of surgical aggregation across various real-world setups by varying the following factors:

1. Number of Participating Clients (K)
2. Label Heterogeneity (ψ)
3. Dataset Size (N)

We used the baseline deep learning model that was trained using the entire NIH dataset and complete disease label representation to establish an upper bound for model performance. This allowed us to evaluate all the approaches on the held-out NIH test set containing all disease labels.

Across all three factors, each client's contributions to the complete data and disease label representation become sparse and model convergence becomes significantly harder to achieve. Our results demonstrate that surgical aggregation consistently outperformed all other approaches on the held-out NIH test set as well as the external MIMIC test set across varying number of clients, label heterogeneity, and dataset size, as illustrated in Figures 2 and 3.

As shown in Figure 2, the performance margin between surgical aggregation and federated learning significantly increased with increase in the number of federated clients (0.06 for $K = 2$ to 0.14 for $K = 10$) as well as increase in label heterogeneity (0 for $\psi = 0$ to 0.12 for $\psi = 1$). Similar results were also observed in the external MIMIC

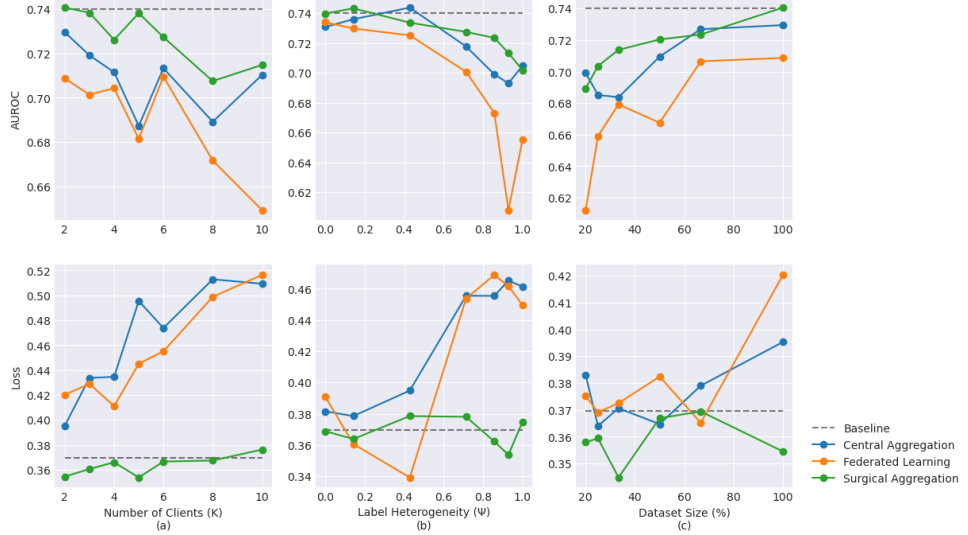


Fig. 3 Model metrics on the external MIMIC test set when evaluating the effect of **(a)** number of clients (K), **(b)** label heterogeneity (ψ), and **(c)** dataset size (N).

test set as shown in Figure 3. These results demonstrate the efficacy of using surgical aggregation for aggregating knowledge from distributed datasets, especially in real-world scenarios with large number of clients and diverse disease labels. Detailed breakdown of model performance, along with p-values for statistical significance, is provided in Extended Data Tables 1, 2, 3. Disease-level model performance is visualized in Extended Data Figure 1 with a detailed breakdown provided in Supplementary Section 2.

Overall, our results indicate that surgical aggregation provides a significant improvement in model performance compared to central aggregation and federated learning. Across varying number of participating clients, surgical aggregation yields a mean AUROC of 0.81 ± 0.01 on the held-out NIH test set, compared to central aggregation (0.78 ± 0.02 , $p = 0.004$) and federated learning (0.71 ± 0.05 , $p < 0.001$). Similarly, on the external MIMIC test set, surgical aggregation has better generalizability with a mean AUROC of 0.73 ± 0.01 compared to central aggregation (0.71 ± 0.01 , $p = 0.02$) and federated learning (0.69 ± 0.02 , $p = 0.001$). Across varying label heterogeneity, surgical aggregation yields a mean AUROC of 0.80 ± 0.01 on the held-out NIH test set, compared to central aggregation (0.79 ± 0.02 , $p = 0.01$) and federated learning (0.74 ± 0.01 , $p = 0.01$). Similarly, on the external MIMIC test

set, surgical aggregation has better generalizability with a mean AUROC of 0.73 ± 0.01 compared to central aggregation (0.72 ± 0.02 , $p = 0.17$) and federated learning (0.69 ± 0.04 , $p = 0.004$). Across varying label heterogeneity, surgical aggregation yields a mean AUROC of 0.80 ± 0.01 on the held-out NIH test set, compared to central aggregation (0.79 ± 0.02 , $p = 0.01$) and federated learning (0.74 ± 0.01 , $p = 0.01$). Similarly, on the external MIMIC test set, surgical aggregation has better generalizability with a mean AUROC of 0.73 ± 0.01 compared to central aggregation (0.72 ± 0.02 , $p = 0.17$) and federated learning (0.69 ± 0.04 , $p = 0.004$).

Harmonization of NIH and CheXpert datasets

While the results from the analytical experiments using synthetic iid datasets indicate that surgical aggregation outperforms other strategies, it is crucial to demonstrate its ability to harmonize real-world non-iid distributed datasets. In this experiment, we surgically aggregate the NIH and CheXpert datasets to train a 20 disease label classifier. Unlike the initial experiments, the complete disease label representation is not available and, as a result, model performance is measured by the performance of each model on held-out test sets from the NIH and CheXpert datasets, in addition to the external MIMIC test set. However, we can

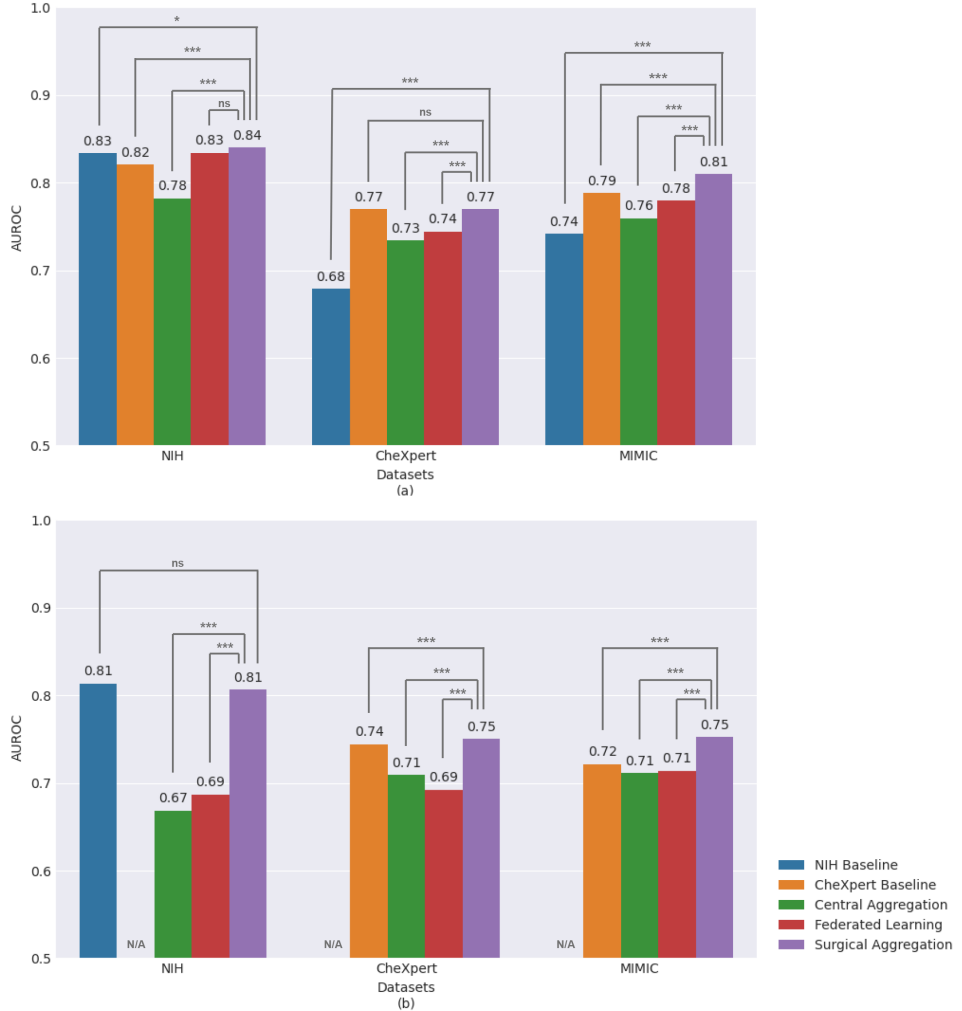


Fig. 4 Mean AUROC scores on held-out NIH and CheXpert test sets and external MIMIC test set across (a) the seven shared labels and (b) all observed disease labels.
 $(* p < 0.05, ** p < 0.01, *** p < 0.001)$

still establish an upper bound for model performance by training baseline models separately on the NIH and CheXpert datasets. We evaluate the performance of each model across (1) the seven shared labels between the NIH and CheXpert dataset and (2) all the observed 20 labels.

For the seven shared disease labels, the surgical aggregation model classified the held-out NIH test set with a mean AUROC of 0.84, significantly better than the NIH baseline model (mean AUROC = 0.83, $p = 0.02$) and the CheXpert baseline model (mean AUROC = 0.82, $p < 0.001$). Similarly, the surgical aggregation model classified the CheXpert test set with a mean

AUROC of 0.77, comparable to the CheXpert baseline model (mean AUROC = 0.77, $p = 0.98$), but significantly better than the NIH baseline model (mean AUROC = 0.68, $p < 0.001$). Furthermore, surgical aggregation outperformed all other approaches across both test sets ($p < 0.001$) with the exception of federated learning on the held-out NIH test set ($p = 0.07$). On the external MIMIC test set, we observe that the surgical aggregation model generalizes better than the baseline models and the other approaches with a mean AUROC of 0.81 ($p < 0.001$). While the difference in model performance across all models may be minimal for seven shared disease

labels, the superiority of surgical aggregation is clearly demonstrated when all the observed disease labels are considered. On the held-out NIH test set, surgical aggregation performs comparably to the NIH baseline with a mean AUROC of 0.81 ($p = 0.06$), while outperforming both central aggregation and federated learning ($p < 0.001$). On the held-out CheXpert test set, surgical aggregation outperforms the CheXpert baseline model and all other approaches with a mean AUROC of 0.75 ($p < 0.001$). Similarly, we observe that surgical aggregation outperforms all baseline models, central aggregation, and federated learning on the external MIMIC test set with a mean AUROC of 0.75 ($p < 0.001$). Figure 4 illustrates the performance of all the approaches across both shared-labels and all-label evaluations. As shown in Figure 4, the performance of the surgical aggregation model across the two evaluations had a performance margin of 0.03, significantly lower compared to 0.11 for central aggregation and 0.14 for federated learning. These results indicate the potential bias in the performance of federated learning and central aggregation models towards shared labels as opposed to the unshared labels between the two datasets. Detailed breakdown of model performance, along with p-values for statistical significance, is provided in Extended Data Table 4. Disease-level model performance is visualized in Extended Data Figure 2 with detailed breakdown provided in Supplementary Section 3.

Discussion

Although the release of large-scale CXR datasets has spearheaded the utility of deep learning models, the distributed nature of these datasets have limited their clinical utility. Our results demonstrate the utility of surgical aggregation in harmonizing and leveraging non-iid, heterogeneous and distributed datasets with partial labels in aggregate to train clinically useful models. Furthermore, our results indicate that surgically aggregated global models, not only tackle domain shift with non-iid data, but also result in better generalizability on external datasets.

Across all analytical experiments, we observe that surgical aggregation scales well to different federated setups with varying data and disease label heterogeneity, while outperforming centrally aggregated and federated learning models. We

observe similar findings when surgically aggregating the NIH and CheXpert datasets. Surgical aggregation demonstrates a significant leap in model performance when all disease labels are considered while generalizing better to unseen distributions. We believe this is a combination of two effects: (1) unlike the other two approaches, surgical aggregation is less susceptible to degrading model performance due to sparse and varying client contributions, and (2) surgical aggregation is able to learn a generalized distribution across diverse datasets and tasks. These findings are in stark contrast to observations regarding models trained using central aggregation and federated learning. Firstly, both approaches result in degrading model performance due to the presence of partial labels. While model performance on the seven shared labels is close, albeit inferior, to the performance of surgical aggregation, when all the 20 observed disease labels are considered, the difference is striking. Unlike surgical aggregation, we observe that central aggregation and federated learning result in a significant degradation of performance on disease labels not shared across participating clients, thus resulting in a significantly worse overall model performance. Finally, our results indicate that central aggregation is prone to resulting in a model biased towards the data with greater contributions. We observe that the centrally aggregated model learned an unequal distribution biased towards the larger CheXpert dataset and thus, resulting in a significantly worse performance on the NIH dataset.

To that end, our work demonstrates how surgical aggregation can leverage large-scale, distributed, non-iid medical imaging datasets with diverse tasks in aggregate to train clinically-useful global models through semi-supervised data harmonization. More importantly, our work emphasizes the importance of greater multi-institutional collaboration to train robust models, while reducing the barrier to entry for hospitals without existing AI infrastructure, as AI-assisted disease characterization becomes a prevalent in the clinical workflow – a step forward towards bridging the gap from bench to bedside.

Methods

Surgical Aggregation

We developed surgical aggregation as a semi-supervised, model and task-agnostic framework for surgically, i.e. selectively, aggregating task-specific weights learned by all participating clients into the global model at the end of each federated round. Let's consider K participating clients with L_1, L_2, \dots, L_K diseases labels. By utilizing surgical aggregation, the global model can learn and predict the presence of all $\bigcup_{k=1}^K L_k$ observed disease labels. Despite contributing to the global model, each participating client does not need to be aware of other clients or their contributions. In other words, a client can simply choose to contribute knowledge for its client-specific tasks from its training data without interacting with any other client, or may choose to import knowledge for different diagnostic tasks via the global model.

We initialized our surgical aggregation setup as a multi-task and multi-label deep neural network composed of a central server and multiple clients. The model consists of two distinct blocks: (1) a representation block and (2) a task block. In such a setup, the representation block learns a generalized global representation of the data using extracted feature semantics while the task block learns to interpret this representation and predict the presence of abnormalities. During the training phase, the weights of layers corresponding to the representation block are always aggregated from each client at the central server using a predefined `ClientUpdate` and `ServerUpdate` strategies and redistributed back to the clients, thereby learning a generalized representation of the data distribution block. On the other hand, the weights from each task block are surgically aggregated to harmonize and aggregate task-related knowledge from each client into a global task block. If a disease label is shared across one or more clients, the weight and bias applied to the input of the neuron corresponding to that label in each client's task block is aggregated using a predefined surgical aggregation strategy `TaskBlockUpdate`. However, if a disease label is not shared across any other client, the weight and bias remains unchanged. This enables the selective aggregation of the weights applied to the input of the task

block construct a global task block with the ability to classify across all observed disease labels. The surgical aggregation framework is described in detail in Algorithm 1.

Datasets

NIH Chest X-Ray 14

The NIH dataset [4] consists of 14 disease labels with $N = 112,120$ frontal-view CXRs from $M = 30,805$ patients. We randomly divided the dataset into training (70%, $N = 78,571$, $M = 21,563$), validation (10%, $N = 11,219$, $M = 3,080$), and testing (20%, $N = 22,330$, $M = 6,162$) splits while ensuring no patient appears in more than one split. Furthermore, we sampled two synthetic iid toy datasets, NIH (1) and (2), from the NIH dataset by equally distributing patients diagnosed with at least one positive finding with healthy patients to prevent patient overlap. Both synthetic datasets consisted of the same number of patients with distinct training ($M = 10,781$) and validation ($M = 1,540$) sets sampled from the global splits, while ensuring there is no patient overlap.

CheXpert

The Stanford CheXpert dataset [1] consists of 13 disease labels, where seven are shared with the NIH dataset, with $N=224,316$ CXRs from $M=65,240$ patients. Since our study focuses on a multi-label setup, we dropped the label for normal in our analyses. To handle uncertain labels in the dataset, we chose the U-Zeros approach i.e. treating all uncertain labels as negatives. We randomly divided the dataset into training (70%, $N = 155,470$, $M = 45,178$), validation (10%, $N = 22,736$, $M = 6,454$), and testing (20%, $N = 45,208$, $M = 12,908$) splits while ensuring no patient appears in more than one split.

MIMIC-CXR-JPG

To evaluate the generalizability of our methods, we utilized the entire MIMIC-CXR-JPG dataset [2, 27] as our external test set. Similar to the CheXpert dataset, the MIMIC dataset consists of 13 disease labels, where seven are shared with the NIH dataset, with $N = 377,110$ CXRs from 65,379 patients. Since our study focuses on a multi-label setup, we dropped the label for normal in our analyses. To handle uncertain labels

Algorithm 1: Surgical Aggregation

Input: K clients indexed by k with local labels L_k ,
Model layers indexed by l ,
Initialized model parameters $w_{0,k}^{(i)}$,
Training epochs before aggregation E ,
Total federated rounds N ,
Weight aggregation strategy **ClientUpdate** and **ServerUpdate**,
Surgical aggregation strategy **TaskBlockUpdate**;

$L_{global} \leftarrow \bigcup_{k=1}^K L_k$
for each round $n = 1, 2, \dots, N$ **do**
 for each client k and each layer l **do**
 $w_{n,k}^{(l)} \leftarrow \text{ClientUpdate}(l, w_{n-1,k}^{(l)})$
 end
 if $mod(n, E) = 0$ **then**
 for each client k and each layer l **do**
 if layer l is not **TaskBlock** **then**
 $w_{n,k}^{(l)} \leftarrow \text{ServerUpdate}(K, l, w_n^{(l)})$
 else
 for $i \leftarrow 1$ to length of L_{global} **do**
 $w_{agg} \leftarrow []$
 for each client k **do**
 if $L_{global}[i]$ is in L_k **then**
 append $w_n^{(l)}$ to w_{agg}
 end
 end
 $w_{n,k}^{(l)}[:, i] \leftarrow \text{TaskBlockUpdate}(w_{agg})$
 end
 end
 end
 end
end

in the dataset, we chose the U-Zeros approach i.e. treating all uncertain labels as negatives.

Deep Learning Setups

In our study, we utilized the DenseNet121 model architecture [28] to train a multi-label classifier using TensorFlow 2.8.1. All models were trained on CXRs downsampled to 224×224 resolution and normalized between 0 and 1 with data augmentations and learning rate of 5e-5.

Surgical Aggregation

We implemented the surgical aggregation framework with the final fully-connected Dense layer acting as the task block. We utilized FedFBN

[10] to define weight aggregation strategies **ClientUpdate** and **ServerUpdate**. As a result, we initialized our model architecture using pre-trained ImageNet [29] weights, warmed-up classification heads for all participating clients prior to federation using transfer learning, and kept all batch normalization layers frozen during federation. Finally, we performed surgical aggregation on the final classification Dense layer, where **TaskBlockUpdate** would aggregate and average the weights for each disease label. In other words, if more than one client contributed knowledge for a disease label, the weights would be averaged across the contributions of each client.

To compare the performance of surgical aggregation, we trained the following multi-label classifiers using data contributed by all participating clients in aggregate with the presence of partial annotations:

Central Aggregation

The central aggregations strategy involves the training of a model in a centralized setup, where all the contributing data is assumed to be locally available. Despite the previously discussed limitations of this method, centrally training a model on multiple datasets in aggregate is a common practice to train robust and well generalizable models [8, 9, 11, 26]

Federated Learning

We use a modified federated learning strategy to train a global model across distributed data with partial annotations. We assume that all contributing data is distributed identically to the surgical aggregation setup and we utilize FedFBN [10] for model weight aggregation. However, no surgical aggregation is performed. To tackle partial annotations, we utilize a modified binary cross-entropy (BCE) loss function to calculate the partial loss at each client using only the client-specific disease labels. While each local model will optimize model performance on observed disease labels, this approach has an additional overhead of requiring all participating clients to know about other clients and their contributions.

For all experiments, we utilized the DenseNet121 model architecture [28] to train a multi-label classifier using TensorFlow 2.8.1. All models were trained on CXRs downsampled to 224×224 resolution and normalized between 0 and 1 with data augmentations and learning rate of 5e-5. The surgical aggregation and federated learning models were trained with a batch size of 64 using an initial learning rate of 5e-5 for 150 epochs with 1 epoch between two consecutive communication rounds ($E = 1$) and early stopping after 25 epochs with no improvement. At the end of each communication round, local losses from each participating clients were communicated back to the central server and the best performing global model was determined by the model with smallest mean loss. Similarly, the centrally aggregated models were trained with

the same hyperparameters in a centralized setup, assuming all the data is locally available.

Model Metrics and Statistical Significance

Across all experiments, we measured model performance using binary cross-entropy (BCE) loss and the area under the receiver operating characteristic curve (AUROC). In a multi-label scenario, the AUROC score is defined as the mean AUROC score across all disease labels. Furthermore, we calculated the 95% confidence interval (CI) for the AUROC scores and compared one-vs-all using bootstrapping and a paired two-tailed t-test. We defined statistical significance for all experiments as $p < 0.05$.

Experimental setup

In this work, we evaluated surgical aggregation for the detection of abnormalities in CXRs using distributed heterogeneous data with partial annotations across the following two experiments:

Analytical experiments with synthetic iid datasets

In the first experiment, we sampled synthetic iid datasets from the large-scale NIH dataset by equally distributing patients diagnosed with at least one positive finding with healthy patients to prevent patient overlap. The size of each synthetic dataset was determined by the number of participating clients (K) while ensuring all synthetic datasets considered of the same number of patients with distinct training and validation sets without any patient overlap. More specifically, for a K -client setup, the NIH training and validation sets were divided into K groups with random sampling with each training set consisting of $M = \lfloor \frac{21,563}{K} \rfloor$ patients and each validation set consisting of $M = \lfloor \frac{3,080}{K} \rfloor$ patients. Furthermore, to simulate label heterogeneity, we randomly pruned disease labels from each synthetic datasets while ensuring the global model learns knowledge for all 14 disease labels in the NIH dataset.

The motivation behind this setup was to provide the complete disease label representation via the NIH dataset while each synthetic dataset provided a glimpse into it. This enabled us to establish an upper bound for model performance

by training a baseline model on the complete NIH dataset and allowed us to evaluate on the held-out NIH test set containing all disease labels, in addition to seven labels shared with the external MIMIC test set. While the goal of this experiment is not to compare with the baseline model, it still provides valuable insight into the impact of data and label heterogeneity. More importantly, using these synthetic iid datasets, we simulated scenarios with distributed data with partial labels to explore the scalability of surgical aggregation across various setups in the real-world by varying the following factors:

1. **Number of Participating Clients (K):** In our experimentation, as the number of participating clients increase, the data becomes increasingly heterogeneous and individual client contributions become sparse. We compared the performance of surgical aggregation with resultant models from central aggregation and federated learning across seven runs with $K = 2, 3, 4, 5, 6, 8, 10$.
2. **Label Heterogeneity (ψ):** To evaluate the effect of label heterogeneity on surgical aggregation, we compared the performance of the surgically aggregated model with the other models across increasing label heterogeneity. In this work, we define label heterogeneity (ψ) as the proportion of labels not shared by the clients. For example, $\psi = 0$ is equivalent to every client contributing knowledge for the same disease labels, while $\psi = 1$ refers to no disease labels being shared by any client. Furthermore, $\psi = 0$ is the best-case scenario. Consequently, all three methods are equivalent and we can expect similar performance. We evaluated the effect of label heterogeneity in a four-client ($K = 4$) setup across seven runs with $\psi = 0, \frac{2}{14}, \frac{6}{14}, \frac{10}{14}, \frac{12}{14}, \frac{13}{14}, 1$.
3. **Dataset Size (N):** While the first two factors evaluated the effect of data and label heterogeneity on surgical aggregation, we evaluate the effect of dataset sizes with constant data and label heterogeneity. This will enable us to pin-point whether the source of possible model degradation was due to heterogeneity or simply a smaller training set. With a constant

two-client ($K = 2$) setup and label heterogeneity $\psi = \frac{4}{14}$, we evaluate the impact of varying dataset size across six runs with $N = \frac{1}{10}, \frac{1}{8}, \frac{1}{6}, \frac{1}{4}, \frac{1}{3}, \frac{1}{2}$.

Disease label distributions for this experiment are provided in Supplementary Section 1.

Harmonization of NIH and CheXpert datasets

While the analytical experiments using synthetic iid datasets provide invaluable insight into the scalability of surgical aggregation across varying setups, they do not reflect a real-world scenario with large-scale non-iid datasets. Out of all the possible scenarios accounted for our study, tackling distributed non-iid data with partial annotations is the most complex problem due to significant domain shift. In this experiment, we utilize surgical aggregation to harmonize and aggregate the NIH and CheXpert datasets to train a 20 disease label classifier. This is equivalent to a two-client ($K = 2$) setup with label heterogeneity $\psi = \frac{7}{20} (\approx 35\%)$. During training, we utilize differential learning rates $1e-5$ and $5e-5$ for the NIH and CheXpert datasets respectively. However, unlike the analytical experiments, the complete representation of all 20 disease labels is not available. Consequently, we measure model performance individually on the held-out NIH and CheXpert test sets, in addition to the external MIMIC dataset. Additionally, we cross-evaluate the NIH baseline model on the CheXpert test set and vice versa. With these evaluations, we measure two distinct result: the performance of the models on (1) the seven disease labels shared by the NIH and CheXpert datasets and (2) all the 20 observed disease labels. This was motivated to analyse the efficacy of surgical aggregation on the knowledge shared among datasets as well as the knowledge not shared.

Supplementary information

This manuscript is accompanied by a single supplementary materials file containing supplementary sections 1-3 and tables 1-22.

Declarations

Some journals require declarations to be submitted in a standardised format. Please check the Instructions for Authors of the journal to which you are submitting to see if you need to complete this section. If yes, your manuscript must contain the following sections under the heading 'Declarations':

- **Funding:** N/A
- **Competing interests:** No competing interests
- **Ethics approval:** N/A
- **Consent to participate:** N/A
- **Consent for publication:** N/A
- **Data availability:** In our study, three publicly available datasets were used for analysis.
 - **NIH Chest X-Ray 14:** No restrictions, in public domain, <https://arxiv.org/abs/1705.02315>, <https://nihcc.app.box.com/v/ChestX-ray-NIHCC/folder/36938765345>
 - **CheXpert:** Restricted under Stanford University Dataset Research Use Agreement due to patient health data privacy, <https://stanfordmlgroup.github.io/competitions/chexpert>
 - **MIMIC-CXR-JPG:** Restricted under PhysioNet Credentialled Health Data License 1.5.0 due to patient health data privacy, <https://physionet.org/content/mimic-cxr-jpg/2.0.0>
- **Code availability:** Code used in this study is available under the GNU General Public License v3.0 on <https://github.com/UM2ii/SurgicalAggregation>

References

- [1] Irvin, J., Rajpurkar, P., Ko, M., Yu, Y., Ciurea-Ilcus, S., Chute, C., Marklund, H., Haghgoo, B., Ball, R., Shpanskaya, K., *et al.*: CheXpert: A large chest radiograph dataset with uncertainty labels and expert comparison. In: Proceedings of the AAAI Conference on Artificial Intelligence, vol. 33, pp. 590–597 (2019)
- [2] Johnson, A.E., Pollard, T.J., Greenbaum, N.R., Lungren, M.P., Deng, C.-y., Peng, Y., Lu, Z., Mark, R.G., Berkowitz, S.J., Horng, S.: Mimic-cxr-jpg, a large publicly available database of labeled chest radiographs. arXiv preprint arXiv:1901.07042 (2019)
- [3] Nguyen, H.Q., Lam, K., Le, L.T., Pham, H.H., Tran, D.Q., Nguyen, D.B., Le, D.D., Pham, C.M., Tong, H.T., Dinh, D.H., *et al.*: Vindr-cxr: An open dataset of chest x-rays with radiologist's annotations. Scientific Data **9**(1), 1–7 (2022)
- [4] Wang, X., Peng, Y., Lu, L., Lu, Z., Bagheri, M., Summers, R.M.: Chestx-ray8: Hospital-scale chest x-ray database and benchmarks on weakly-supervised classification and localization of common thorax diseases. In: Proceedings of the IEEE Conference on Computer Vision and Pattern Recognition, pp. 2097–2106 (2017)
- [5] Guan, H., Liu, M.: Domain adaptation for medical image analysis: a survey. IEEE Transactions on Biomedical Engineering **69**(3), 1173–1185 (2021)
- [6] Castro, D.C., Walker, I., Glocker, B.: Causality matters in medical imaging. Nature Communications **11**(1), 3673 (2020)
- [7] Kilim, O., Olar, A., Joó, T., Palicz, T., Pollner, P., Csabai, I.: Physical imaging parameter variation drives domain shift. Scientific Reports **12**(1), 21302 (2022)
- [8] Pooch, E.H., Ballester, P., Barros, R.C.: Can we trust deep learning based diagnosis? the impact of domain shift in chest radiograph classification. In: Thoracic Image Analysis: Second International Workshop, TIA 2020, Held in Conjunction with MICCAI 2020, Lima, Peru, October 8, 2020, Proceedings 2, pp. 74–83 (2020). Springer
- [9] Yao, L., Prosky, J., Covington, B., Lyman, K.: A strong baseline for domain adaptation and generalization in medical imaging. arXiv

preprint arXiv:1904.01638 (2019)

- [10] Kulkarni, P., Kanhere, A., Yi, P.H., Parekh, V.S.: Optimizing federated learning for medical image classification on distributed non-iid datasets with partial labels. arXiv preprint arXiv:2303.06180 (2023)
- [11] Cohen, J.P., Hashir, M., Brooks, R., Bertrand, H.: On the limits of cross-domain generalization in automated x-ray prediction. In: Medical Imaging with Deep Learning, pp. 136–155 (2020). PMLR
- [12] Chowdhury, A., Kassem, H., Padoy, N., Umeton, R., Karargyris, A.: A review of medical federated learning: Applications in oncology and cancer research. In: International MICCAI Brainlesion Workshop, pp. 3–24 (2022). Springer
- [13] Rieke, N., Hancox, J., Li, W., Milletari, F., Roth, H.R., Albarqouni, S., Bakas, S., Galtier, M.N., Landman, B.A., Maier-Hein, K., *et al.*: The future of digital health with federated learning. NPJ digital medicine **3**(1), 1–7 (2020)
- [14] Sheller, M.J., *et al.*: Federated learning in medicine: facilitating multi-institutional collaborations without sharing patient data. Scientific Reports **10**(12598) (2020) <https://doi.org/10.1038/s41598-020-69250-1>
- [15] Arasteh, S.T., Isfort, P., Saehn, M., Mueller-Franzes, G., Khader, F., Kather, J.N., Kuhl, C., Nebelung, S., Truhn, D.: Collaborative training of medical artificial intelligence models with non-uniform labels. arXiv preprint arXiv:2211.13606 (2022)
- [16] Gong, X., Sharma, A., Karanam, S., Wu, Z., Chen, T., Doermann, D., Innanje, A.: Ensemble attention distillation for privacy-preserving federated learning. In: Proceedings of the IEEE/CVF International Conference on Computer Vision, pp. 15076–15086 (2021)
- [17] Gong, X., Song, L., Vedula, R., Sharma, A., Zheng, M., Planche, B., Innanje, A., Chen, T., Yuan, J., Doermann, D., *et al.*: Federated learning with privacy-preserving ensemble attention distillation. IEEE Transactions on Medical Imaging (2022)
- [18] Kulkarni, P., Kanhere, A., Yi, P.H., Parekh, V.S.: From competition to collaboration: Making toy datasets on kaggle clinically useful for chest x-ray diagnosis using federated learning. arXiv preprint arXiv:2211.06212 (2022)
- [19] Li, X., Jiang, M., Zhang, X., Kamp, M., Dou, Q.: Fedbn: Federated learning on non-iid features via local batch normalization. arXiv preprint arXiv:2102.07623 (2021)
- [20] Chang, H., Shejwalkar, V., Shokri, R., Houmansadr, A.: Cronus: Robust and heterogeneous collaborative learning with black-box knowledge transfer. arXiv preprint arXiv:1912.11279 (2019)
- [21] Li, D., Wang, J.: Fedmd: Heterogenous federated learning via model distillation. arXiv preprint arXiv:1910.03581 (2019)
- [22] Qu, L., Balachandar, N., Rubin, D.L.: An experimental study of data heterogeneity in federated learning methods for medical imaging. arXiv preprint arXiv:2107.08371 (2021)
- [23] Wang, Y., Shi, Q., Chang, T.-H.: Why batch normalization damage federated learning on non-iid data? arXiv preprint arXiv:2301.02982 (2023)
- [24] Ioffe, S., Szegedy, C.: Batch normalization: Accelerating deep network training by reducing internal covariate shift. In: International Conference on Machine Learning, pp. 448–456 (2015). pmlr
- [25] McMahan, B., *et al.*: Communication-Efficient Learning of Deep Networks from Decentralized Data. In: Proceedings of the 20th International Conference on Artificial Intelligence and Statistics. Proceedings of Machine Learning Research, vol. 54, pp. 1273–1282. PMLR, ??? (2017)
- [26] Seyyed-Kalantari, L., Zhang, H., McDermott,

M.B., Chen, I.Y., Ghassemi, M.: Underdiagnosis bias of artificial intelligence algorithms applied to chest radiographs in under-served patient populations. *Nature medicine* **27**(12), 2176–2182 (2021)

- [27] Goldberger, A.L., Amaral, L.A., Glass, L., Hausdorff, J.M., Ivanov, P.C., Mark, R.G., Mietus, J.E., Moody, G.B., Peng, C.-K., Stanley, H.E.: Physiobank, physioto toolkit, and physionet: components of a new research resource for complex physiologic signals. *circulation* **101**(23), 215–220 (2000)
- [28] Huang, G., *et al.*: Densely connected convolutional networks. *Proceedings of the IEEE conference on computer vision and pattern recognition* (2017) <https://doi.org/10.48550/arXiv.1608.06993>
- [29] Deng, J., Dong, W., Socher, R., Li, L.-J., Li, K., Fei-Fei, L.: Imagenet: A large-scale hierarchical image database. In: *2009 IEEE Conference on Computer Vision and Pattern Recognition*, pp. 248–255 (2009). Ieee

Extended Data

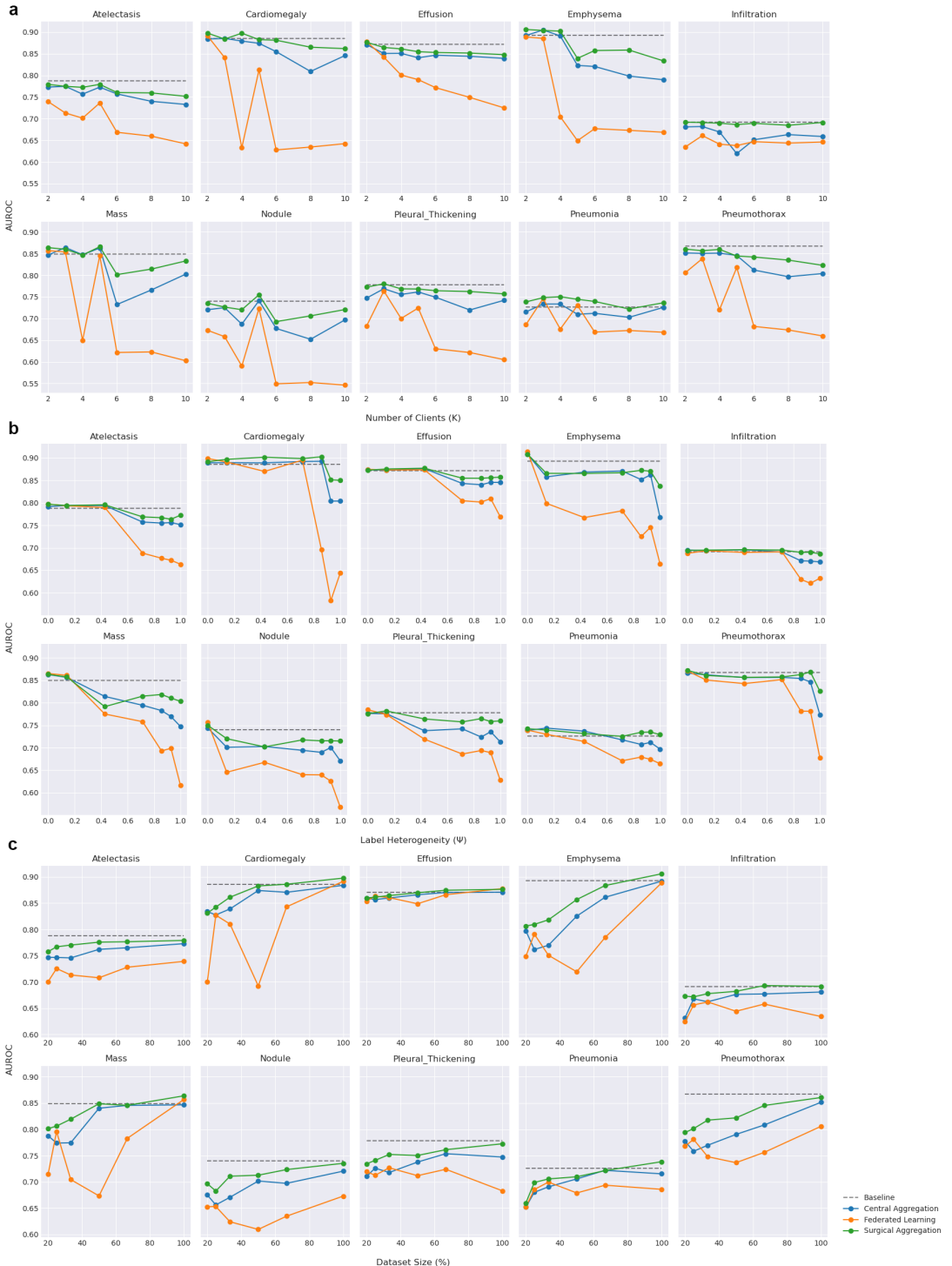


Fig. 1 Disease-level AUROC scores on the held-out NIH test set when evaluating the effect of **(a)** number of clients (K), **(b)** label heterogeneity (ψ), and **(c)** dataset size (N).

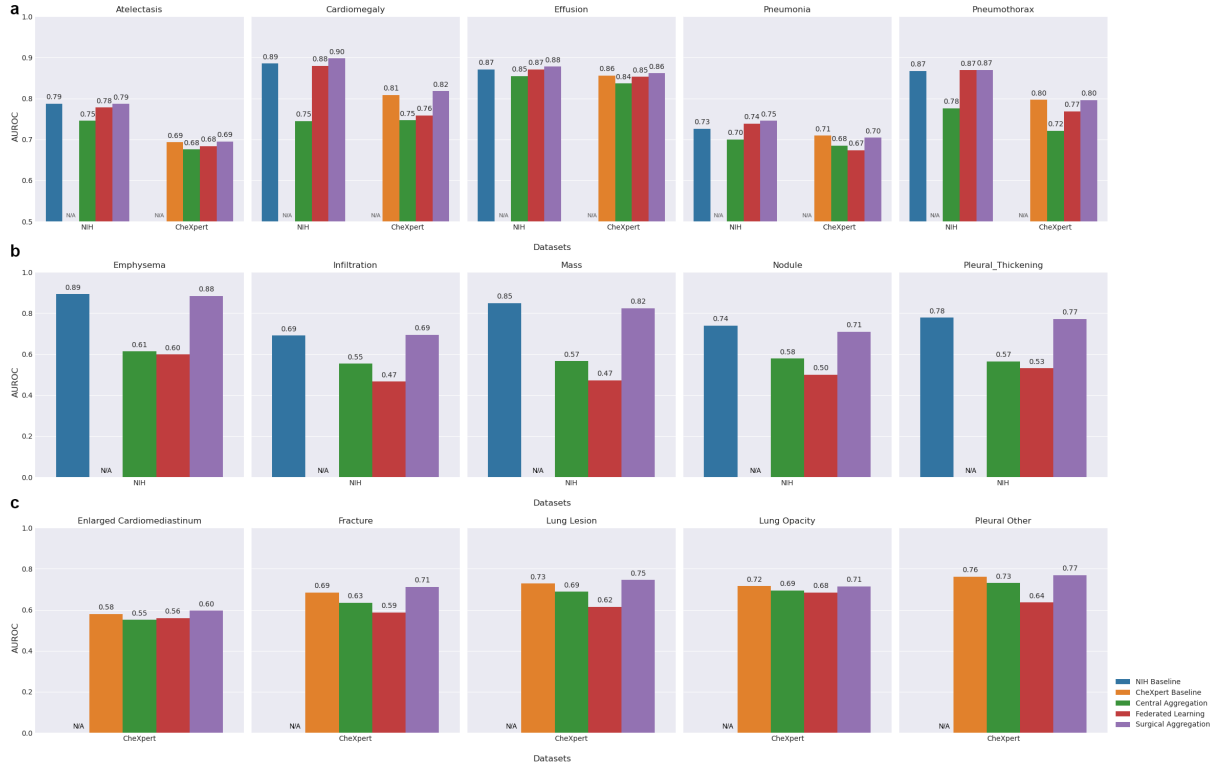


Fig. 2 (a) Disease-level AUROC scores for shared disease labels on the held-out NIH and CheXpert test sets. (b) Disease-level AUROC scores for NIH disease labels not shared with the CheXpert dataset on the held-out NIH test set. (c) Disease-level AUROC scores for CheXpert disease labels not shared with the NIH dataset on the held-out CheXpert test set.

Table 1 Model metrics for analyzing the effect of number of clients (K) on the held-out NIH test set and external MIMIC test set. 95% CI for mean AUROC scores provided in brackets with p-values for statistical significance. Best performing models across each experiment are highlighted in bold.

Model	NIH			MIMIC-CXR		
	Loss	AUROC	p-value	Loss	AUROC	p-value
K = 2						
NIH Baseline	0.15	0.81 [0.81, 0.82]	0.44	0.37	0.74 [0.74, 0.74]	0.41
Central Aggregation	0.16	0.80 [0.80, 0.81]	<0.001	0.40	0.73 [0.73, 0.73]	<0.001
Federated Learning	0.21	0.76 [0.75, 0.77]	<0.001	0.42	0.71 [0.71, 0.71]	<0.001
Surgical Aggregation	0.15	0.82 [0.81, 0.82]	-	0.35	0.74 [0.74, 0.74]	-
K = 3						
NIH Baseline	0.15	0.81 [0.81, 0.82]	0.31	0.37	0.74 [0.74, 0.74]	0.003
Central Aggregation	0.17	0.80 [0.80, 0.81]	0.001	0.43	0.72 [0.72, 0.72]	<0.001
Federated Learning	0.21	0.78 [0.77, 0.78]	<0.001	0.43	0.70 [0.70, 0.70]	<0.001
Surgical Aggregation	0.15	0.82 [0.81, 0.82]	-	0.36	0.74 [0.73, 0.74]	-
K = 4						
NIH Baseline	0.15	0.81 [0.81, 0.82]	0.31	0.37	0.74 [0.74, 0.74]	<0.001
Central Aggregation	0.18	0.79 [0.79, 0.80]	0.005	0.43	0.71 [0.71, 0.71]	<0.001
Federated Learning	0.23	0.69 [0.68, 0.70]	<0.001	0.41	0.70 [0.70, 0.71]	<0.001
Surgical Aggregation	0.15	0.81 [0.81, 0.82]	-	0.37	0.73 [0.73, 0.73]	-
K = 5						
NIH Baseline	0.15	0.81 [0.81, 0.82]	0.07	0.37	0.74 [0.74, 0.74]	0.007
Central Aggregation	0.19	0.79 [0.78, 0.79]	<0.001	0.50	0.69 [0.69, 0.69]	<0.001
Federated Learning	0.22	0.74 [0.74, 0.75]	<0.001	0.45	0.68 [0.68, 0.68]	<0.001
Surgical Aggregation	0.15	0.81 [0.80, 0.81]	-	0.35	0.74 [0.74, 0.74]	-
K = 6						
NIH Baseline	0.15	0.81 [0.81, 0.82]	<0.001	0.37	0.74 [0.74, 0.74]	<0.001
Central Aggregation	0.20	0.77 [0.77, 0.78]	<0.001	0.47	0.71 [0.71, 0.71]	<0.001
Federated Learning	0.22	0.66 [0.65, 0.67]	<0.001	0.46	0.71 [0.71, 0.71]	<0.001
Surgical Aggregation	0.16	0.80 [0.79, 0.80]	-	0.37	0.73 [0.73, 0.73]	-
K = 8						
NIH Baseline	0.15	0.81 [0.81, 0.82]	<0.001	0.37	0.74 [0.74, 0.74]	<0.001
Central Aggregation	0.22	0.75 [0.74, 0.76]	<0.001	0.51	0.69 [0.69, 0.69]	<0.001
Federated Learning	0.24	0.66 [0.65, 0.66]	<0.001	0.50	0.67 [0.67, 0.67]	<0.001
Surgical Aggregation	0.16	0.80 [0.79, 0.80]	-	0.37	0.71 [0.71, 0.71]	-
K = 10						
NIH Baseline	0.15	0.81 [0.81, 0.82]	<0.001	0.37	0.74 [0.74, 0.74]	<0.001
Central Aggregation	0.21	0.75 [0.74, 0.75]	<0.001	0.51	0.71 [0.71, 0.71]	<0.001
Federated Learning	0.23	0.65 [0.64, 0.66]	<0.001	0.52	0.65 [0.65, 0.65]	<0.001
Surgical Aggregation	0.16	0.79 [0.78, 0.80]	-	0.38	0.72 [0.71, 0.72]	-

Table 2 Model metrics for analyzing the effect of label heterogeneity (ψ) on the held-out NIH test set and external MIMIC test set. 95% CI for mean AUROC scores provided in brackets with p-values for statistical significance. Best performing models across each experiment are highlighted in bold.

Model	NIH			MIMIC-CXR		
	Loss	AUROC	p-value	Loss	AUROC	p-value
$\Psi = 0$						
NIH Baseline	0.15	0.81 [0.81, 0.82]	0.003	0.37	0.74 [0.74, 0.74]	<0.001
Central Aggregation	0.15	0.82 [0.81, 0.82]	0.05	0.38	0.73 [0.73, 0.73]	0.14
Federated Learning	0.15	0.82 [0.82, 0.83]	0.95	0.39	0.73 [0.73, 0.73]	<0.001
Surgical Aggregation	0.15	0.82 [0.82, 0.83]	-	0.37	0.74 [0.74, 0.74]	-
$\Psi = 2/14$						
NIH Baseline	0.15	0.81 [0.81, 0.82]	0.34	0.37	0.74 [0.74, 0.74]	<0.001
Central Aggregation	0.15	0.82 [0.81, 0.82]	0.63	0.38	0.74 [0.73, 0.74]	<0.001
Federated Learning	0.19	0.80 [0.79, 0.80]	<0.001	0.36	0.73 [0.73, 0.73]	<0.001
Surgical Aggregation	0.15	0.82 [0.81, 0.82]	-	0.36	0.74 [0.74, 0.75]	-
$\Psi = 6/14$						
NIH Baseline	0.15	0.81 [0.81, 0.82]	0.14	0.37	0.74 [0.74, 0.74]	<0.001
Central Aggregation	0.16	0.81 [0.80, 0.81]	0.53	0.39	0.74 [0.74, 0.74]	<0.001
Federated Learning	0.19	0.77 [0.76, 0.77]	<0.001	0.34	0.72 [0.72, 0.72]	<0.001
Surgical Aggregation	0.15	0.81 [0.80, 0.81]	-	0.38	0.73 [0.73, 0.74]	-
$\Psi = 10/14$						
NIH Baseline	0.15	0.81 [0.81, 0.82]	<0.001	0.37	0.74 [0.74, 0.74]	<0.001
Central Aggregation	0.18	0.79 [0.78, 0.79]	<0.001	0.46	0.72 [0.73, 0.72]	<0.001
Federated Learning	0.21	0.74 [0.73, 0.75]	<0.001	0.45	0.70 [0.70, 0.70]	<0.001
Surgical Aggregation	0.15	0.80 [0.79, 0.81]	-	0.38	0.73 [0.73, 0.73]	-
$\Psi = 12/14$						
NIH Baseline	0.15	0.81 [0.81, 0.82]	<0.001	0.37	0.74 [0.74, 0.74]	<0.001
Central Aggregation	0.19	0.78 [0.77, 0.78]	<0.001	0.46	0.70 [0.70, 0.70]	<0.001
Federated Learning	0.22	0.70 [0.69, 0.70]	<0.001	0.47	0.67 [0.67, 0.67]	<0.001
Surgical Aggregation	0.15	0.80 [0.79, 0.80]	-	0.36	0.72 [0.72, 0.72]	-
$\Psi = 13/14$						
NIH Baseline	0.15	0.81 [0.81, 0.82]	<0.001	0.37	0.74 [0.74, 0.74]	<0.001
Central Aggregation	0.19	0.77 [0.77, 0.78]	<0.001	0.47	0.69 [0.69, 0.69]	<0.001
Federated Learning	0.21	0.69 [0.68, 0.70]	<0.001	0.46	0.61 [0.61, 0.61]	<0.001
Surgical Aggregation	0.15	0.79 [0.78, 0.80]	-	0.35	0.71 [0.71, 0.71]	-
$\Psi = 1$						
NIH Baseline	0.15	0.81 [0.81, 0.82]	<0.001	0.37	0.74 [0.74, 0.74]	<0.001
Central Aggregation	0.20	0.75 [0.75, 0.76]	<0.001	0.46	0.70 [0.70, 0.70]	<0.001
Federated Learning	0.22	0.66 [0.65, 0.67]	<0.001	0.45	0.66 [0.65, 0.66]	<0.001
Surgical Aggregation	0.16	0.78 [0.77, 0.79]	-	0.37	0.70 [0.70, 0.70]	-

Table 3 Model metrics for analyzing the effect of dataset size (N) on the held-out NIH test set and external MIMIC test set. 95% CI for mean AUROC scores provided in brackets with p-values for statistical significance. Best performing models across each experiment are highlighted in bold.

Model	NIH			MIMIC-CXR		
	Loss	AUROC	p-value	Loss	AUROC	p-value
$N = 1/10$						
NIH Baseline	0.15	0.81 [0.81, 0.82]	<0.001	0.37	0.74 [0.74, 0.74]	<0.001
Central Aggregation	0.17	0.75 [0.74, 0.76]	0.002	0.38	0.70 [0.70, 0.70]	<0.001
Federated Learning	0.19	0.72 [0.71, 0.72]	<0.001	0.38	0.61 [0.61, 0.61]	<0.001
Surgical Aggregation	0.16	0.76 [0.76, 0.77]	-	0.36	0.69 [0.69, 0.69]	-
$N = 1/8$						
NIH Baseline	0.15	0.81 [0.81, 0.82]	<0.001	0.37	0.74 [0.74, 0.74]	<0.001
Central Aggregation	0.17	0.75 [0.74, 0.76]	<0.001	0.36	0.69 [0.68, 0.69]	<0.001
Federated Learning	0.19	0.75 [0.74, 0.75]	<0.001	0.37	0.66 [0.66, 0.66]	<0.001
Surgical Aggregation	0.16	0.77 [0.76, 0.78]	-	0.36	0.70 [0.70, 0.71]	-
$N = 1/6$						
NIH Baseline	0.15	0.81 [0.81, 0.82]	<0.001	0.37	0.74 [0.74, 0.74]	<0.001
Central Aggregation	0.17	0.75 [0.75, 0.76]	<0.001	0.37	0.68 [0.68, 0.69]	<0.001
Federated Learning	0.19	0.74 [0.73, 0.74]	<0.001	0.37	0.68 [0.68, 0.68]	<0.001
Surgical Aggregation	0.16	0.79 [0.78, 0.79]	-	0.34	0.71 [0.71, 0.72]	-
$N = 1/4$						
NIH Baseline	0.15	0.81 [0.81, 0.82]	<0.001	0.37	0.74 [0.74, 0.74]	<0.001
Central Aggregation	0.16	0.78 [0.77, 0.78]	<0.001	0.36	0.71 [0.71, 0.71]	<0.001
Federated Learning	0.20	0.71 [0.70, 0.71]	<0.001	0.38	0.67 [0.67, 0.67]	<0.001
Surgical Aggregation	0.15	0.80 [0.79, 0.80]	-	0.37	0.72 [0.72, 0.72]	-
$N = 1/3$						
NIH Baseline	0.15	0.81 [0.81, 0.82]	0.004	0.37	0.74 [0.74, 0.74]	<0.001
Central Aggregation	0.16	0.79 [0.78, 0.80]	<0.001	0.38	0.73 [0.73, 0.73]	<0.001
Federated Learning	0.19	0.75 [0.74, 0.76]	<0.001	0.37	0.71 [0.71, 0.71]	<0.001
Surgical Aggregation	0.15	0.80 [0.80, 0.81]	-	0.37	0.72 [0.72, 0.72]	-
$N = 1/2$						
NIH Baseline	0.15	0.81 [0.81, 0.82]	0.44	0.37	0.74 [0.74, 0.74]	0.41
Central Aggregation	0.16	0.80 [0.80, 0.81]	<0.001	0.40	0.73 [0.73, 0.73]	<0.001
Federated Learning	0.21	0.76 [0.75, 0.77]	<0.001	0.42	0.71 [0.71, 0.71]	<0.001
Surgical Aggregation	0.15	0.82 [0.81, 0.82]	-	0.35	0.74 [0.74, 0.74]	-

Table 4 Model metrics on held-out NIH and CheXpert test sets and external MIMIC test set. 95% CI for mean AUROC scores provided in brackets with p-values for statistical significance. Best performing models are highlighted in bold.

(a) Seven Shared Disease Labels

Model	NIH			CheXpert			MIMIC-CXR		
	Loss	AUROC	p-value	Loss	AUROC	p-value	Loss	AUROC	p-value
NIH Baseline	0.15	0.83 [0.83, 0.84]	0.02	0.73	0.68 [0.68, 0.68]	<0.001	0.37	0.74 [0.74, 0.74]	<0.001
CheXpert Baseline	0.22	0.82 [0.82, 0.83]	<0.001	0.41	0.77 [0.77, 0.77]	0.98	0.30	0.79 [0.79, 0.79]	<0.001
Central Aggregation	0.22	0.78 [0.78, 0.79]	<0.001	0.44	0.73 [0.73, 0.74]	<0.001	0.31	0.76 [0.76, 0.76]	<0.001
Federated Learning	0.18	0.83 [0.83, 0.84]	0.07	0.44	0.74 [0.74, 0.75]	<0.001	0.28	0.78 [0.77, 0.78]	<0.001
Surgical Aggregation	0.15	0.84 [0.84, 0.85]	-	0.41	0.77 [0.77, 0.77]	-	0.26	0.81 [0.81, 0.81]	-

(b) All Disease Labels

Model	NIH			CheXpert			MIMIC-CXR		
	Loss	AUROC	p-value	Loss	AUROC	p-value	Loss	AUROC	p-value
NIH Baseline	0.15	0.81 [0.81, 0.82]	0.06	-	-	-	-	-	-
CheXpert Baseline	-	-	-	0.38	0.74 [0.74, 0.75]	<0.001	0.27	0.72 [0.72, 0.72]	<0.001
Central Aggregation	0.28	0.67 [0.66, 0.68]	<0.001	0.39	0.70 [0.70, 0.71]	<0.001	0.28	0.71 [0.71, 0.71]	<0.001
Federated Learning	0.23	0.68 [0.67, 0.69]	<0.001	0.44	0.69 [0.68, 0.69]	<0.001	0.27	0.71 [0.71, 0.72]	<0.001
Surgical Aggregation	0.15	0.81 [0.81, 0.81]	-	0.38	0.75 [0.75, 0.75]	-	0.25	0.75 [0.75, 0.75]	-